

PRECISE LOCALIZATION OF FLUORESCENT PROBES WITHOUT NUMERICAL FITTING

Sean B. Andersson

Aerospace and Mechanical Eng., Boston University, Boston, MA 02215

ABSTRACT

A new algorithm for determining the location of a fluorescent probe in the plane is described. Inspired by the Bancroft algorithm for localization in the global positioning system, the technique calculates the position of the probe without the use of a numerical fitting procedure. Numerical simulations are presented which indicate that the precision of the localization is similar to that obtained using the standard method of fitting a Gaussian profile to the measured fluorescence intensity. Moreover, the computational time is two orders of magnitude shorter than when performing such a fit.

Keywords: biomedical microscopy, biomedical imaging

1. INTRODUCTION

The resolution of a visible light microscope is limited to approximately half the wavelength of the light [1]. An object smaller than this appears as a diffraction-limited spot. While the structural details of such an object cannot be distinguished, its location can be determined with much higher accuracy by finding the center of the image spot. The fluorescence intensity measured at a given location depends on the distance to the fluorescent probe and therefore a collection of measurements obtained at different locations (e.g. from the pixels in a charge-coupled device (CCD) image) can be interpreted as a set of range-only measurements taken at different locations in space. The problem of determining position from a set of range-only measurements occurs in many settings. One notable example is the problem of position determination using the global positioning system (GPS). Several algorithms have been developed to solve the GPS positioning problem, including a closed form solution known as Bancroft's algorithm [2]. In this paper we present a method based on Bancroft's algorithm for localizing a fluorescent probe in the image plane. This algorithm, fluoroBancroft, yields a closed-form solution for the location of the fluorescent probe.

Sub-diffraction-limit localization is typically done by fitting the data to a Gaussian profile using a non-linear least-squares fit [3]. This can provide precision on the order of 1-20 nm [4] and has been used to great effect in single particle tracking and other applications (e.g. [5, 6]). However, it involves a numerical fitting procedure to determine the pa-

rameters in the Gaussian function. While this is not a problem when the data is analyzed off-line, it does impose a limitation for real-time localization. We show in Sec. 4 that the algorithm proposed here is roughly two orders of magnitude faster than the Gaussian fitting approach with only a moderate reduction in localization accuracy.

Bancroft's algorithm yields two possible solutions, only one of which is physical. The fluoroBancroft algorithm presented here follows the same basic approach as the Bancroft algorithm. However, due to the structure of the dependence of the fluorescence intensity on the distance between the measurement location and the position of the fluorescence source, there is only a single solution. A closed-form equation for this solution is derived. This equation involves the pseudo-inverse of a matrix formed from the measured data. As an initial investigation of the fluoroBancroft algorithm, we present a numerical comparison of its performance to that of the non-linear least-squares Gaussian fit using data generated through computer simulation of CCD images of a fluorescent probe.

2. THE FLUROBANCROFT ALGORITHM

The point spread function of a diffraction-limited spot is given by an Airy function [7]. Near the peak, this function is well-approximated by a Gaussian [4]. Since the Gaussian is mathematically more tractable, we choose to model the intensity of a diffraction limited spot by

$$I_{psf} = m e^{-\frac{r^2}{2\sigma^2}}. \quad (1)$$

Here r is the distance between the measurement location and the fluorescent probe, m is a scaling factor determined by the total number of photons emitted by the probe during the measurement period and σ is the full-width, half-maximum (FWHM) of the image spot, given by

$$\sigma = \frac{1.22\lambda}{4\text{N.A.} \ln 2} \quad (2)$$

where N.A. is the numerical aperture of the objective.

The measured intensity is given by the true intensity together with background and shot noise. The background noise, arising from sources such as dark current, sensor noise and autofluorescence of the sample, is assumed to be constant across the field of view. For the purposes of position estimation,

we model it as a Gaussian random variable η_B with mean and variance equal to N_B . The shot noise is a Poisson process with a rate dependent on the total number of photons detected [3]. We assume that the photon count is high enough to model this noise as a Gaussian random variable η_{shot} with mean and variance N_{shot} equal to the sum of the intensity and the expected value of the background noise. The model for the measured intensity at a distance r away from the probe is

$$I = me^{-\frac{r^2}{2\sigma^2}} + \eta_B + \eta_{shot}. \quad (3)$$

Taking the expected value of (3) and solving for r yields

$$r^2 = 2\sigma^2 \ln(2m) - 2\sigma^2 \ln(I - 2N_B). \quad (4)$$

Note that because the background noise can be measured, the second term on the right-hand side of (4) is known. However m is related to the true intensity of the fluorophores on the probe and is therefore not known. Let i index the measurements obtained from the (known) positions (x_i, y_i) . The range can be expressed as $r_i^2 = (x_i - x_0)^2 + (y_i - y_0)^2$ where (x_0, y_0) is the (unknown) true location of the fluorescent probe. Define

$$\begin{aligned} b &\triangleq 2\sigma^2 \ln(2m), & P_i^2 &\triangleq 2\sigma^2 \ln(I - 2N_B) \\ \alpha_i &\triangleq \frac{1}{2} (x_i^2 + y_i^2 + P_i^2), & \Lambda &\triangleq \frac{1}{2} (x_0^2 + y_0^2). \end{aligned}$$

Then (4) can be rewritten as

$$0 = \alpha_i + \Lambda - \begin{pmatrix} x_i & y_i & 1 \end{pmatrix} \begin{pmatrix} x_0 \\ y_0 \\ b \end{pmatrix}. \quad (5)$$

Stacking together n measurements yields

$$0 = \alpha + \Lambda e - B \begin{pmatrix} x_0 \\ y_0 \\ b \end{pmatrix} \quad (6)$$

where

$$\alpha = \begin{pmatrix} \alpha_1 \\ \vdots \\ \alpha_n \end{pmatrix}, \quad e = \begin{pmatrix} 1 \\ \vdots \\ 1 \end{pmatrix}, \quad B = \begin{pmatrix} x_1 & y_1 & 1 \\ & \vdots & \\ x_n & y_n & 1 \end{pmatrix}.$$

Pre-multiplying (6) by B^T and rearranging yields

$$\begin{pmatrix} x_0 & y_0 & b \end{pmatrix} = B^\dagger (\alpha + \Lambda e) \quad (7)$$

where $B^\dagger = (B^T B)^{-1} B^T$ is the pseudo-inverse of B . Notice that the unknown position (x_0, y_0) appears both on the left-hand side and on the right-hand side (through Λ). We now state an interesting property of B^\dagger which can be shown using a direct calculation of the pseudoinverse.

Proposition 2.1 *Let $e = (1, 1, \dots, 1)^T$ and let A be an $n \times 2$ matrix. Define $B = \begin{pmatrix} A & e \end{pmatrix}$. Then*

$$B^\dagger e = \begin{pmatrix} 0 & 0 & 1 \end{pmatrix}^T.$$

To apply this proposition, define

$$Q = \begin{pmatrix} 1 & 0 & 0 \\ 0 & 1 & 0 \end{pmatrix}.$$

Then

$$\begin{pmatrix} x_0 \\ y_0 \end{pmatrix} = Q \begin{pmatrix} x_0 \\ y_0 \\ b \end{pmatrix} = Q (B^\dagger (\alpha + \Lambda e)) = QB^\dagger \alpha. \quad (8)$$

Since B and α depend only on the measurements and the locations of those measurements, (8) determines the location of the fluorescent probe as a closed-form equation.

The measurement model (3) is not valid for large r (with respect to σ). Including measurements from too far away will therefore degrade the performance of the algorithm. To mitigate this, we discard all measurements lower than a threshold defined as follows. The parameter m can be estimated by integrating (1) and setting it equal to the total number of photons collected in the image minus the expected value of the background noise. The threshold is then set to $I_{thresh} = me^{-2}$.

3. METHODS

To investigate the performance of the fluoroBancroft algorithm, we developed a simulation similar to that described in [3]. We modeled a point source fluorescing at a wavelength of 540 nm and imaged through an objective lens with an N.A. of 1.2 onto a CCD. The PSF was modeled as a Gaussian and the pixel size in the CCD image was taken to be 100 nm. To obtain the noise-free intensity values, the PSF was integrated over each pixel. Background noise was introduced by adding a sample from a Poisson distribution with parameter $N_B = 10$ photons. Finally shot noise was introduced by adding a sample from a Poisson distribution with parameter given by the sum of the PSF across the pixel and the background noise value. An example image for a 16×16 pixel array is shown in Fig. 1. The origin is at the center of the image while the true location of the probe is at (50 nm, 50 nm).

The signal-to-noise ratio (SNR) in an image was defined as in [8] to be

$$\text{SNR} = \frac{I_0}{\sqrt{N_B + \sigma_{I_0}^2}} \quad (9)$$

where N_B is the variance of the background noise, I_0 is the maximum signal intensity above background, and $\sigma_{I_0}^2$ is the experimentally determined variance of the maximum signal intensity. To vary the SNR, simulations were run with a range of different fluorescence intensities (corresponding to either different integration times or excitation intensities). 1000 iterations were run for each intensity. The location of the particle in an image was determined using the fluoroBancroft algorithm described in Sec. 2 as well as by using a nonlinear

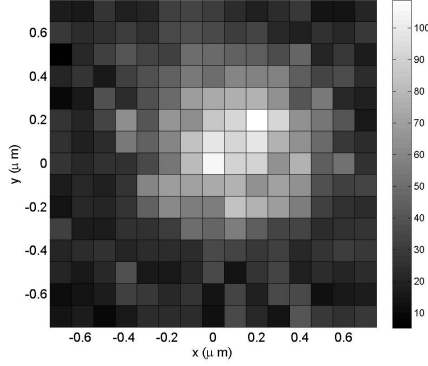


Fig. 1. Simulated CCD image for a 16×16 pixel array with a fluorescent probe at $(x, y) = (50 \text{ nm}, 50 \text{ nm})$. It fluoresced at a rate of 4 photons/ms. The background rate was 10 photons/sec/pixel and the integration time was 500 ms. The corresponding SNR was 11. Grey level indicates the number of photons collected.

least-squares fit of the data to a Gaussian given by

$$I(x, y) = Ae^{-\frac{(x-x_0)^2+(y-y_0)^2}{2\sigma^2}}$$

in which x_0, y_0, A and σ were allowed to vary. The simulations were performed in Matlab and the Gaussian fit performed using the built-in routine `lsqnonlin`.

4. RESULTS AND DISCUSSION

To compare the computational complexity, the average time to compute the location of the fluorescent probe using both algorithms was calculated. The results are shown in Fig. 2 in which the ratio of the time for the Gaussian fit to the time for the fluoroBancroft algorithm is shown for three different sizes of pixel arrays. Because Matlab is typically slower than a custom program, the exact times are not meaningful. However, the ratio provides a rough measure of the relative computational complexity. For all these simulations, the fluoroBancroft algorithm was at least 50 times faster and generally more than two orders of magnitude faster than the Gaussian fit. The calculation of the estimate using the fluoroBancroft algorithm from (8) grows linearly in complexity with the number of measurements but is independent of the SNR. By contrast the Gaussian fit is done through numerical optimization and thus the computation time depends on the initial condition, the amount of data, the SNR, and the tolerance desired.

Fig. 3 shows the mean absolute error and standard deviation of the two algorithms as a function of SNR for three different sizes of pixel arrays. For the 16×16 pixel array, the Gaussian fit outperforms the fluoroBancroft algorithm, though both provide a precision well below the diffraction limit. One factor in the performance of the new algorithm is the choice of the threshold for including a measurement (see Sec. 2). Data

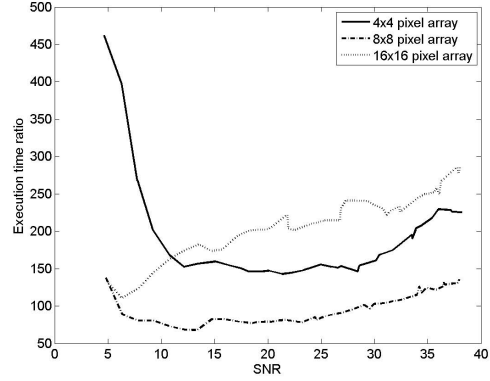


Fig. 2. Ratio of execution time of Gaussian fit to fluoroBancroft for a range of SNR and pixel array sizes.

from pixels far from the location of the probe are not well-modeled by (3) and skew the estimate. It is likely that the performance of the fluoroBancroft algorithm can be improved by using a more detailed approach for determining the threshold or a more detailed measurement model. As the pixel array size decreases (as for a finely focused spot or for large pixel sizes), all the pixels contain a strong signal from the probe. For the smallest pixel array, the fluoroBancroft algorithm outperforms the Gaussian fit technique. For all array sizes, the performance of the algorithms is quite similar at higher SNR.

There are several applications for which the speed of the fluoroBancroft algorithm will be beneficial. It is possible to track a large number of fluorescent probes in a wide-field image simultaneously (see, e.g. [9]). To achieve tracking of all the probes in real-time, it is necessary that the algorithm used be as fast as possible. By tracking in real-time, it would be possible to adjust parameters such as light intensity or to add chemicals to the sample based on the position of the molecules. Another interesting application is real-time tracking of a fluorescing probe using a confocal or multi-photon microscope [10–12]. In this setting, the data points are acquired sequentially and it is therefore beneficial to localize the probe with a smaller number of measurements. Moreover, we are currently extending the algorithm to provide a closed-form solution to the localization problem in three-dimensions.

5. ACKNOWLEDGEMENTS

The author thanks P.S. Krishnaprasad for his personal notes on and for discussions about the Bancroft algorithm in GPS.

6. REFERENCES

- [1] J. E. N. Jonkman and E. H. K. Stelzer, “Resolution and contrast in confocal and two-photon microscopy,” in *Confocal and two-photon microscopy: Foundations*,

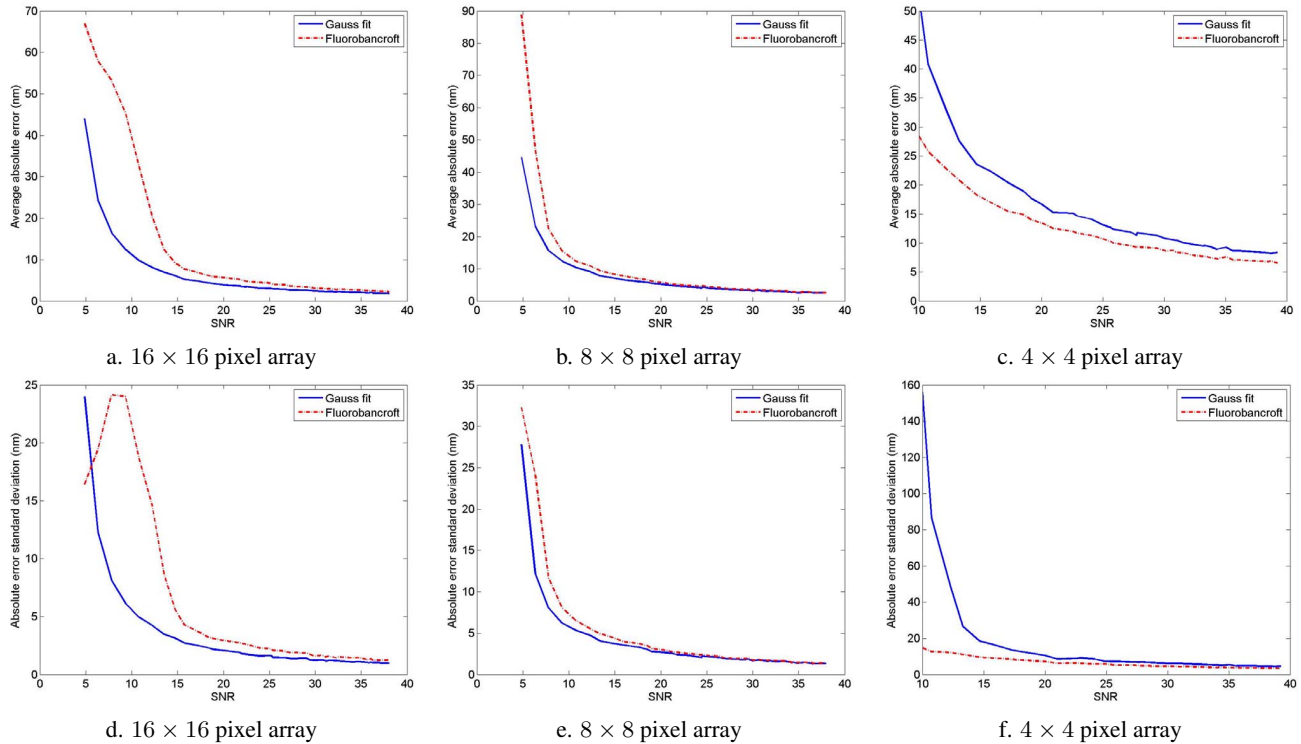


Fig. 3. Mean absolute error and standard deviation of the location estimates of the fluoroBancroft (dash-dot) and Gaussian fit (solid) algorithms for a range of SNR and pixel array sizes. The Gaussian fit outperforms fluoroBancroft for large pixel arrays while fluoroBancroft yields better results for small pixel arrays. In each case, the performance of the two algorithms is comparable at higher SNR.

applications, and advances, A. Diaspro, Ed. Wiley-Liss, 2002, ch. 5, pp. 101–126.

- [2] S. Bancroft, “An algebraic solution of the GPS pseudo-range equations,” *IEEE Trans. Aerosp. Electron. Syst.*, vol. AES-21, pp. 56–59, November 1985.
- [3] M. K. Cheezum, W. F. Walker, and W. H. Guilford, “Quantitative comparison of algorithms for tracking single fluorescent particles,” *Biophys. J.*, vol. 81, pp. 2378–2388, 2001.
- [4] R. E. Thompson, D. R. Larson, and W. W. Webb, “Precise nanometer localization analysis for individual fluorescent probes,” *Biophys. J.*, vol. 82, pp. 2775–2783, 2002.
- [5] C. Kural, H. Balci, and P. R. Selvin, “Molecular motors one at a time: FIONA to the rescue,” *J. Phys. Condens. Matter*, vol. 17, pp. S3979–S3995, 2005.
- [6] M. Lakadamyali, M. J. Rust, H. P. Babcock, and X. Zhuang, “Visualizing infection of individual influenza viruses,” *P. Natl. Acad. Sci. USA*, vol. 100, pp. 9280–9285, 2003.
- [7] R. Juškaitis, *The Handbook of Biological Confocal Microscopy*, 3rd ed. Springer, 2006, ch. 11. Measuring the real point spread function of high numerical aperture microscope objective lenses, pp. 239–250.
- [8] U. Kubitschek, O. Kückmann, T. Kues, and R. Peters, “Imaging and tracking of single GFP molecules in solution,” *Biophys. J.*, vol. 78, pp. 2170–2179, April 2000.
- [9] A. Geonvesio, T. Liedl, V. Emiliani, W. J. Parak, M. Copepy-Moisan, and J.-C. Olivo-Marin, “Multiple particle tracking in 3-d+t microscopy: method and application to the tracking of endocytosed quantum dots,” *IEEE Trans. Image Processing*, vol. 15, no. 5, pp. 1062–1070, 2006.
- [10] A. J. Berglund and H. Mabuchi, “Tracking-FCS: Fluorescence correlation spectroscopy of individual particles,” *Opt. Express*, vol. 13, no. 20, pp. 8069–8082, 2005.
- [11] S. B. Andersson, “Tracking a single fluorescent molecule with a confocal microscope,” *Appl. Phys. B*, vol. 80, no. 7, pp. 809–816, 2005.
- [12] T. Ragan, H. Huang, P. So, and E. Gratton, “3D particle tracking on a two-photon microscope,” *J. Fluoresc.*, vol. 16, no. 3, pp. 325–336, 2006.